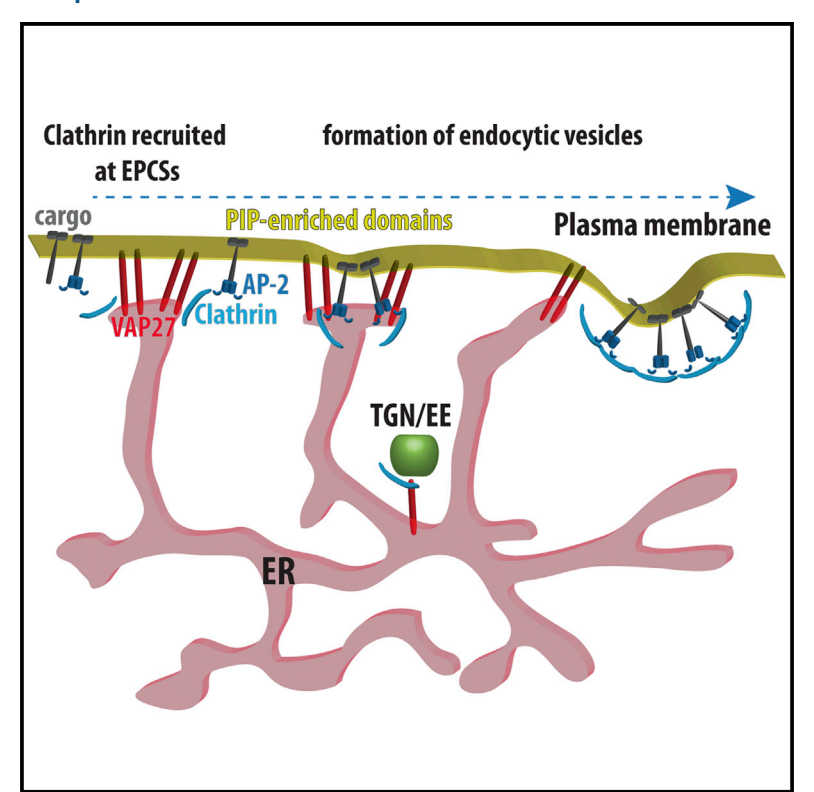
Cell Reports

Plant Endocytosis Requires the ER Membrane-Anchored Proteins VAP27-1 and VAP27-3

Graphical Abstract



Authors

Giovanni Stefano, Luciana Renna, Clarissa Wormsbaecher, Jessie Gamble, Krzysztof Zienkiewicz, Federica Brandizzi

Correspondence

fb@msu.edu

In Brief

Stefano et al. demonstrate that plant VAPs (VAP27-1 and VAP27-3) interact with clathrin and with phosphatidylinositol-phosphate lipids (PIPs) that populate endocytic membranes. The findings support a model showing that, through interaction with PIPs and clathrin, VAP27-proteins bridge the ER with endocytic membranes and maintain endocytic traffic.

Highlights

- VAP27-1 and VAP27-3 interact with clathrin in vitro and in vivo
- VAP27-1 and VAP27-3 interact with lipids enriched in endocytic membranes
- VAP27-1 and VAP27-3 are required for endocytosis and plant growth
- The loss of VAP27-proteins alters homeostasis of the endocytic membranes







Plant Endocytosis Requires the ER Membrane-Anchored Proteins VAP27-1 and VAP27-3

Giovanni Stefano,^{1,2} Luciana Renna,¹ Clarissa Wormsbaecher,^{1,3} Jessie Gamble,¹ Krzysztof Zienkiewicz,^{1,4} and Federica Brandizzi^{1,2,5,*}

¹MSU-DOE Plant Research Lab, Michigan State University, East Lansing, MI 48824, USA

²Plant Biology Department, Michigan State University, East Lansing, MI 48824, USA

³Present address: Department of Molecular Genetics, Ohio State University, Columbus, OH 43210, USA

⁴Present address: Department of Plant Biochemistry, Georg-August-University, Albrecht-von-Haller-Institute for Plant Sciences, Göttingen 37073, Germany

⁵Lead Contact

*Correspondence: fb@msu.edu

https://doi.org/10.1016/j.celrep.2018.04.091

SUMMARY

Through yet-undefined mechanisms, the plant endoplasmic reticulum (ER) has a critical role in endocytosis. The plant ER establishes a close association with endosomes and contacts the plasma membrane (PM) at ER-PM contact sites (EPCSs) demarcated by the ER membrane-associated VAMP-associated-proteins (VAP). Here, we investigated two plant VAPs, VAP27-1 and VAP27-3, and found an interaction with clathrin and a requirement for the homeostasis of clathrin dynamics at endocytic membranes and endocytosis. We also demonstrated direct interaction of VAP27-proteins with phosphatidylinositolphosphate lipids (PIPs) that populate endocytic membranes. These results support that, through interaction with PIPs, VAP27-proteins bridge the ER with endocytic membranes and maintain endocytic traffic, likely through their interaction with clathrin.

INTRODUCTION

Endocytosis is an essential process (Fan et al., 2013), and clathrin-mediated endocytosis (CME) is a major mechanism controlling the plasma membrane (PM) proteome (Gadeyne et al., 2014). During CME, proteins are recognized by adaptor proteins and packaged into vesicles that bud from endocytic membranes into the cell (McMahon and Boucrot, 2011). CME relies on different steps to assemble vesicles, including the rate-limiting recruitment of clathrin to endocytic membranes, vesicle budding, and uncoating (Robinson, 2015). In addition to PM subdomains, clathrin is associated with subdomains of the *trans*-Golgi network (TGN) (Ito et al., 2012; Konopka et al., 2008), an endosomal cargo-sorting hub in the biosynthetic and endocytic routes (Viotti et al., 2010). How clathrin associates to membrane subdomains is not completely understood, but a role for charged lipids is emerging (McMahon and Boucrot, 2011).

In plants, several endocytic components have been identified (Fan et al., 2015), but little is known about how the endocytic machinery is recruited and regulated on membranes. Intriguingly, the

plant endoplasmic reticulum (ER) associates with endosomes, including the TGN, which in plants functions as an early endosome (EE) (Stefano et al., 2015; Viotti et al., 2010). Disruption of the integrity of the plant ER network and membrane fluidity compromises endocytosis (Stefano et al., 2015). Because the plant ER influences the movement of endocytic organelles, the ER-driven streaming may be necessary for their function (Stefano et al., 2015); however, the ER membrane may have additional roles. Also, although the functional association of ER and endosomes infers that in plant cells endocytosis homeostasis depends on an interaction of the ER with endocytic membranes (Stefano et al., 2015), the underlying mechanisms are yet unknown.

Members of the metazoan and yeast VAMP-associated-protein (VAPs), which are generally type II ER integral proteins, work as tethers between the ER and endosomes (Alpy et al., 2013), and the PM at the ER-PM contact sites (EPCSs) (Stefan et al., 2011). VAP27-1 and VAP27-3, two of the four plant homologs of the non-plant VAPs (Wang et al., 2014), have been localized to the bulk ER and the EPCSs (Saravanan et al., 2009; Wang et al., 2014, 2016). Non-plant VAPs have various cellular functions, including lipid transport and membrane traffic (Lev et al., 2008), but their physiological roles in plants are unknown. The hypothesis for an involvement of plant EPCSs in endocytosis (Wang et al., 2017) and the close association of the ER with the endocytic organelles (Stefano et al., 2015) make VAPs candidates to establish the mechanistic connection between endocytosis and the plant ER. Therefore, in this work, we have investigated the role of VAP27-1 and VAP27-3 in endocytosis. We found that these proteins interact with clathrin and phosphatidylinositol-phosphate lipids (PIPs) and are required for clathrin dynamics at endocytic membranes and for endocytosis integrity. We propose that the VAP27-proteins bridge the ER with endocytic membranes, likely through their interaction with clathrin and PIPs. Such an interaction may facilitate the clathrin targeting and dynamic binding to endocytic membrane subdomains, as well as the ER-driven endosomal movement, which underpin endocytosis homeostasis.

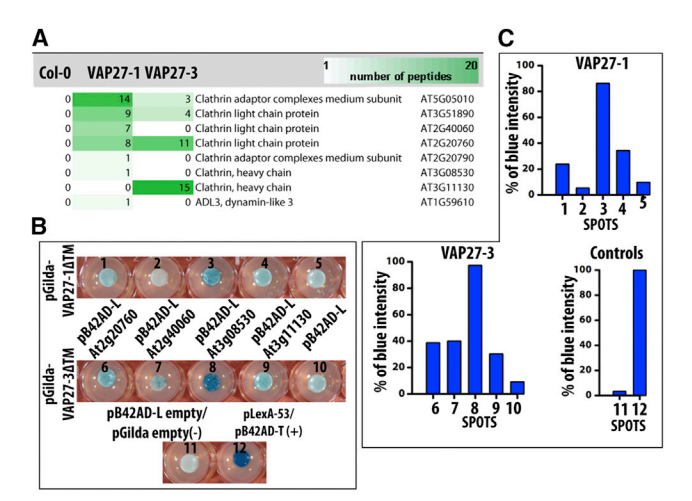
RESULTS

VAP27-Proteins Interact with Clathrin In Vitro

We queried the interactome of VAP27-1 and VAP27-3 by coimmunoprecipitation (coIP) and liquid chromatography-tandem







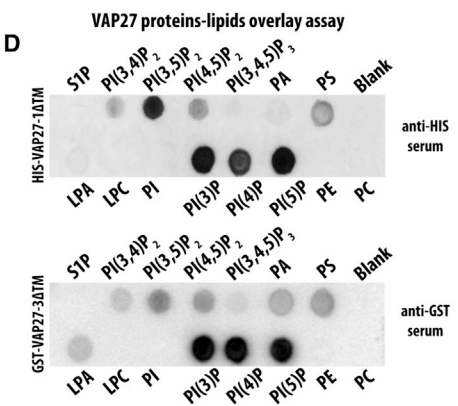


Figure 1. VAP27-1 and VAP27-3 Interact with Clathrin and Bind **Lipids Abundant in Endocytic Membranes**

(A) List of proteins and heatmap of the number of peptides detected by coIP experiments for VAP27-1-YFP and VAP27-3-YFP (0 indicates absence of peptides).

- (B) Y2H assay of the VAP27-cytosolic domain with five of the clathrin proteins identified in the pulldowns (blue color: protein-protein interaction).
- (C) Percentage (%) of blue color intensity (relative to B) compared to the positive control (spot 12 in B showing the degree of protein interaction).
- (D) Protein-lipid overlay assay.

mass spectrometry (LC/MS/MS) in lines stably expressing functional YFP fusions (Wang et al., 2015, 2016). Among the interactors, we found microtubules, already known to interact with VAP27-1 and VAP27-3 (Wang et al., 2014), and proteins involved in endocytosis, namely light and heavy clathrin isoforms, adaptor proteins, and dynamin (Figures 1A and S1A). With a eukaryotic linear motif (ELM) search and clustalW alignment, we identified a conserved clathrin box motif (LLTID/VE) (Figure S1B), which mediates direct protein-clathrin interactions in non-plant species (Puertollano et al., 2001), at the VAP27-proteins N terminus (Figure S1B). Using yeast two-hybrid (Y2H) analysis, we confirmed the interaction of both VAP27-1 and VAP27-3 with clathrin light (CLCs) and heavy chains (CHCs) (Figures 1B and 1C) and, to a much reduced extent, with the clathrin adaptor protein (Figure S1C). The strength of the interaction of each VAP27-protein was different for the CLCs, but similar for the heavy chains CHCs (Figure 1C). Together, these results indicate that VAP-proteins interact, at least indirectly, with the clathrin coat assembling machinery.

VAP27-Proteins Interact Directly with Lipids Enriched in Endocytic Membranes

The non-plant VAP cytosolic domain serves as bridge between the ER and heterotypic membranes (Stefan et al., 2013). We tested whether VAP27-proteins could interact directly with lipids present in biological membranes through protein-lipid overlay assays with a recombinant cytosolic domain of VAP27-1 and VAP27-3. We found a preferential interaction with PI(3)P, PI(4) P, PI(5)P, PI(3,5)P2, PI(4,5)P2, and PI(3,4)P2 (Figure 1D), which are present to different levels in TGN/EEs, late endosomes (LEs), and PM (Simon et al., 2014). Therefore, VAP27-proteins interact directly with a specific subset of lipids that populate endocytic membranes that have been shown to be closely associated with the plant ER (Stefano et al., 2015; Wang et al., 2014).

VAP27-1 and VAP27-3 Transiently Associate with Clathrin In Vivo

We next tested the spatial relationship of clathrin and endocytic membranes with VAP27-proteins. In leaf epidermal cells, VAP27-proteins were localized at the bulk ER and EPCSs (Figures 2A, 3A, and S2) (Wang et al., 2014). The latter co-localized with a small subpopulation of LEs labeled by YFP-RabF2a (Stefano et al., 2015) (Figure S2A). To visualize clathrin, we used a YFP fusion of CHC2 (herein referred as YFP-CHC), which is localized to cytosolic punctate structures of various sizes in plant cells (Ortiz-Morea et al., 2016; Wang et al., 2015). The larger punctate YFP-CHC structures are TGN/EEs, and the smaller ones (diameter \leq 0.25 μ m) are endocytic structures, which are likely foci of clathrin coated pits at the PM or endosomally derived vesicles (Ito et al., 2012; Konopka et al., 2008; Wang et al., 2013, 2015). Here, we collectively indicate the smaller clathrin-coated structures (diameter ≤0.25 μm) asCCSs. Live-cell confocal imaging analyses in leaf epidermal cells confirmed the TGN/EE identity of the CHC-structures with a >0.25 µm diameter (Figure S2B) and the heterogeneous subcellular distribution of YFP-CHC (Figures 2A, S2B, and S3A; Videos S1 and S2).

Using surface plot analyses, which report the pixel intensity values of fluorescent structures as pseudo-colored images in a three-dimensional graph, in cells co-expressing YFP-CHC with either VAP27-1-CFP (Figure 2B) or VAP27-3-CFP (Figure S3B), we correlated the subcellular distribution of the ER network, EPCSs, and CCSs at a spatial scale. The YFP-CHC signal aligned along tracks delineated by the cortical ER network visualized by the fluorescent VAP27-fusions; we also verified an apparently close association of the EPCSs with CCSs (Figures 2B and S3D). To further investigate the relationship of the EPCSs with CCSs, we estimated the percentage of EPCSs associated with CCSs in relation to the total number of EPCSs per area of cell cortex (33 areas, area size: 222.47 μm²). On average, 15% of the total EPCSs were associated with CCSs (Figures 2C, 2D, S3C, and S3D). We next probed the association of EPCSs, which are generally immotile (Wang et al., 2014, 2016) and

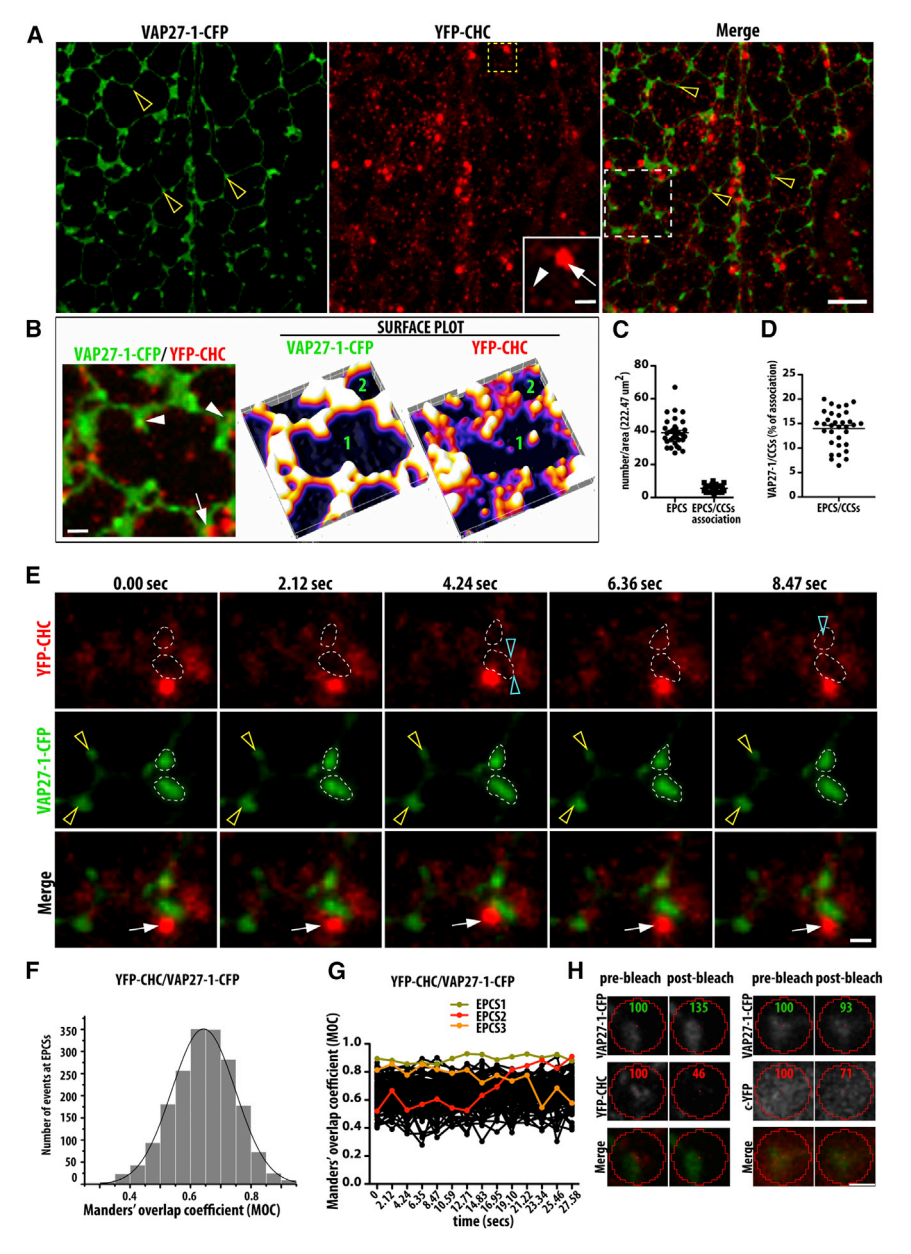


Figure 2. EPCSs and Clathrin Are Transiently Associated

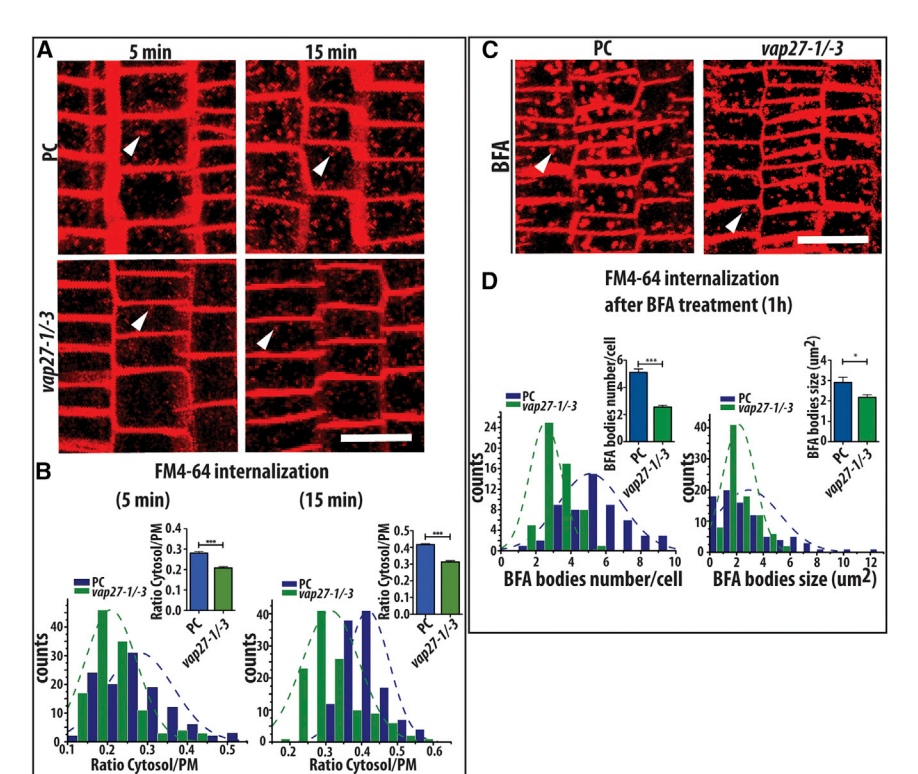
(A) Subcellular distribution of VAP27-1-CFP and YFP-CHC visualized by CLSM of *N. tabacum* leaf epidermal cells. Empty yellow arrows indicate EPCSs. CCSs and TGN/EEs (see also Figure S2) are indicated in the inset and by a white arrowhead and arrow, respectively. Inset: magnified area delineated by a yellow dotted square in main image. Scale bar, 5 µm; inset scale bar, 1 µm.

- (B) Magnified dashed square in merge image of (A) (scale bar, 1 µm), and separate surface plot profiles of this magnified area for VAP27-1-CFP and YFP-CHC signals. The corresponding areas between the two plots are indicated by numbers.
- (C) Graph indicating the number of EPCSs per area $(222.47 \, \mu m^2)$ and the number of EPCSs associated with CCSs per area (n of analyzed areas = 33).
- (D) Percentage of EPCSs labeled by VAP27-1-CFP associated with CCSs (calculated from values in C).
- (E) Confocal images from a high-resolution time-lapse sequence showing a dynamic association of VAP27-1-CFP and YFP-CHC structures. In the YFP-CHC images, dotted circles surround the EPCSs labeled by VAP27-1-CFP (see VAP27-1-CFP panels). Note the dynamic formation of CCSs from a cytosolic pool (light blue arrowhead) or dissolution of CCSs (green arrowhead) in correspondence of the EPCSs. Dashed lines circumscribe the area occupied by two other EPCSs. In the merge panels, arrows indicate one TGN/EE in the sequence. Note the appearance and disappearance of the CHC-associated structures with respect to the VAP27-1-CFP-labeled membranes. Scale bar, 5 μm.
- (F) The degree of co-localization between VAP27-1-CFP and YFP-CHC is expressed as MOC.
- (G) MOC calculated over 27.58 s for 104 EPCSs. Green, red and orange lines are an example of VAP27-1-CFP and YFP-CHC co-localization behavior during 27.58 s.
- (H) Left: positive FRET experiment on VAP27-1-CFP/YFP-CHC. Right: control FRET (VAP27-1-CFP/cytosolic YFP). Numbers in each panel indicate the fluorescence percentage (%).

CCSs, at a temporal scale. High-resolution time-lapse imaging indicated that the association of the CCSs with the EPCSs was transient (Figures 2E and S3D; Videos S1 and S2). Furthermore, in coincidence of the EPCSs, over time the YFP-CHC signal could concentrate into the CCSs or dissolve from a punctate appearance (Figures 2E and S3E; Videos S1 and S2). These observations supported a dynamic association of the EPCSs and CCSs. To validate this, we used two independent quantitative approaches. We estimated the Mander's overlap coefficient (MOC) to evaluate the degree of overlapping fluorescent signals of 156 individual EPCSs labeled by either VAP27-1-CFP or VAP27-3-CFP and the CCSs in 2,184 consecutive snapshots. The MOC values had a Gaussian distribution (Figures 2F and S3E), supporting a dynamic association of the EPCSs with the

CCSs (Figure 2E). Estimation of the MOC values over time for each EPCS indicated that the association of the EPCSs with the CCSs could change. For example, in a 27.58-s time-lapse sequence, the CCSs could be found either continuously or just temporarily associated with EPCSs (Figures 2G and S3F). Such a statistical distribution of the MOC values can be explained based on a formation and dissociation of CCSs at the PM during CME and/or the formation and dissolution of endocytic-derived vesicles in the cytoplasm. To further characterize the association between the EPCSs and CCSs, we used fluorescence resonance energy transfer (FRET) analyses on EPCSs as the CCSs emerged in the focal plane. We found a positive FRET signal on EPCSs labeled by VAP27-CFP proteins and CCSs supporting that EPCS components can interact with CCSs (Figures





2H and S3G). These *in vivo* results validated the proteomics and Y2H analyses for an interaction of clathrin and VAP27-proteins (Figures 1A, 1B, S1A, and S1C). We next tested if the TGN/EEs, which bind clathrin, could also associate with the ER and EPCSs. Consistent with earlier reports (Ueda et al., 2004; Voigt et al., 2005), we found that the TGN/EEs were highly pleomorphic and motile structures in close contact with the ER network (Figures 2 and S3D; Videos S1 and S2). We also verified that the TGN/EEs could be in temporary association with the EPCSs (Figures 2E and S3D, arrows). Together, these results indicate that clathrin-enriched membranes are transiently distributed in the close proximity of the EPCSs and the bulk ER network labeled by VAP27-proteins.

VAP27-1 and VAP27-3 Are Required for Endocytosis and Growth

The verified association between VAP27-proteins with clathrinenriched membranes and PIPs supported the hypothesis that VAP27-proteins could be involved in endocytosis. To test this, we generated a *vap27-1/vap27-3* double mutant, herein dubbed *vap27-1/-3*, through floral crosses of single *VAP27* knockouts (Figures S4A and S4B). The single and double VAP27 mutant showed mild but significant defects in plant growth (Figures S4C–S4F).

By monitoring the internalization of the endocytic tracer FM4-64 in root cortex cells at 5 and 15 min after pulse-labeling in wild-type (WT) (parental control, PC), we found a labeling of endosomal structures within 5 min, which increased over time (Figures 3A and 3B). Internalization of the dye occurred also in *vap27-1/-3*, but the fluorescence levels were significantly lower

Figure 3. Endocytosis Is Delayed in vap27-1/-3

(A) Maximal projections of confocal images showing FM4-64 internalization (5, 15 min) into endosomes (arrowheads) in 6DAG WT and *vap27-1/-3* root cells.

(B) Graphs show fluorescence quantification in the cytosol versus PM (Doyle et al., 2015) at 5 and 15 min (*n* of cells for each genotype and each time point = 119).

(C) Maximal projection image showing BFA bodies in WT and *vap27-1/-3* root cells (arrowheads) upon pulse-labeling with FM4-64 and treatment with 50 uM BFA for 1 hr. Scale bar. 5 um.

(D) Number of BFA bodies per cell (n cells = 56) and size of BFA bodies (n = 87).

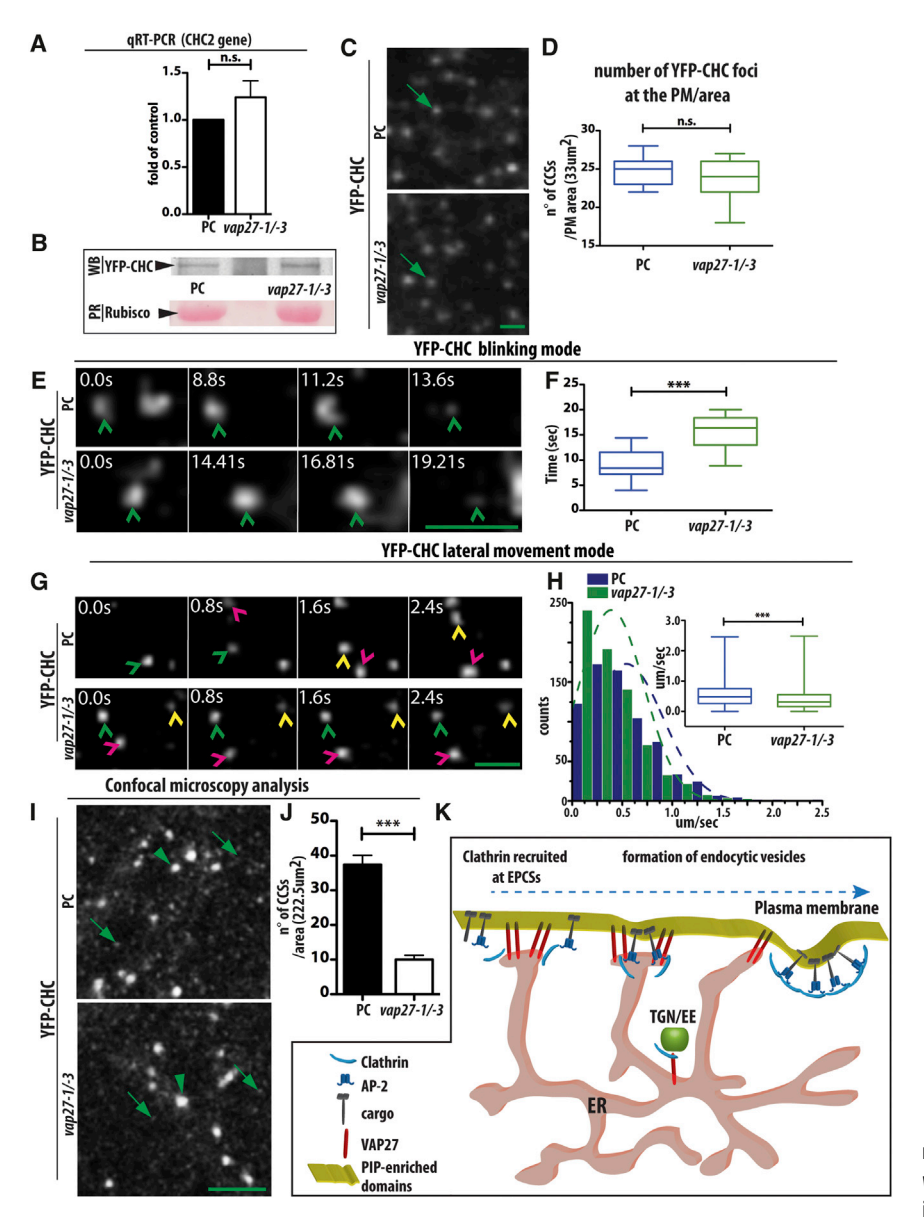
compared to WT (Figures 3A and 3B), supporting a delay in endocytosis in this mutant. Brefeldin A (BFA) compromises exocytic traffic leading to the formation of endosome aggregates, known as BFA bodies (Lam et al., 2009). Endocytosis defects delay the formation of BFA bodies and negatively influence their size (Paciorek et al., 2005). Consistent with the reduced internalization of FM4-64 (Figures 3E and 3F), in the *vap27-1/-3* mutant

the number and size of BFA bodies were lower compared to WT (Figures 3C and 3D). Therefore, the loss of VAP27-1 and VAP27-3 partially compromises endocytosis.

We next investigated whether defects in VAP27 levels could affect the TGN/EE morphology using transmission electron microscopy (TEM) on WT and *vap27-1/-3* cells. We observed significant differences in the Golgi and TGN/EE organization in the VAP27 mutant (Figure S4G). Therefore, the loss of VAP27-proteins partially affects the TGN/EE morphology, consistently with the defects in endocytic traffic verified thus far in the *vap27-1/-3* mutant.

The Loss of VAP27-Proteins Alters the Dynamics of Clathrin and Homeostasis of the Endocytic Membranes

We next tested the distribution of CCSs in WT and vap27-1/-3 using live-cell imaging in lines stably expressing YFP-CHC. We generated isogenic backgrounds through crosses of vap27-1/-3 with a YFP-CHC line, which were confirmed by quantitative analyses of YFP-CHC expression (gRT-PCR) (Figure 4A) and anti-GFP immunoblots (Figure 4B). We assayed whether the cellular availability of VAP27-proteins could influence the dynamic distribution of CCSs at the PM. The visualization of clathrin signal at the PM reflects the formation of clathrin-coated membranes as PM-associated clathrin foci as well as peripheral CCSs distributed in the cytosol in close proximity to the PM. To establish whether the loss of VAP27-protein could affect the number and movement of CCSs near the PM, we performed variable-angle epifluorescence microscopy/total internal reflection fluorescence (VAEM/TIRF) microscopy, which allows visualizing proteins close to the PM in intact plant tissues and has been



used successfully to follow clathrin-coated membranes at the PM (Wan et al., 2011). We found that the number of CCSs/ imaging area in vap27-1/-3 was similar to the control (Figures 4C and 4D); however, the blinking time (time between appearance and disappearance of CCSs at the PM) was significantly reduced in the mutant compared to WT (29% decrease) (Figures 4E and 4F). The lateral movement of the peripheral CCSs was also reduced (28% decrease in the mutant) (Figures 4G and 4H). We then used live-cell confocal microscopy analyses, which enable visualizing a thin layer of cytoplasm (Figure 4I) and capturing both the peripheral CCSs in close association with the PM and the CCSs distributed more distally from the PM. We found that the number of CCSs/confocal area was significantly reduced in vap27-1/-3 compared to WT (Figures 4I and 4J). Because no differences were found in the number of CCSs at the PM (Figure 4D), these results indicate that the

Figure 4. The Loss of VAP27-1 and VAP27-3 Compromises CHC Distribution and Homeostasis of the Endocytic Membranes

(A) qRT-PCR analyses show unchanged levels of *CHC2* expression in PC and *vap27-1/-3*.

(B) Immunoblot analyses of YFP-CHC (~220 kDa) with GFP-antibody on soluble fractions of PC/ YFP-CHC, *vap27-1/-3*/YFP-CHC. Protein loading control (rubisco; Ponceau red [PR] staining).

(C) VAEM/TIRF microscopy of leaf epidermal cells of WT and *vap27-1/-3* stably expressing YFP-CHC. Arrows point to CCS. Scale bar, 1 um.

(D) Number of CCSs (n = 30 areas for each genotype).

(E) VAEM/TIRF microscopy of hypocotyl epidermal cells in WT and *vap27-1/-3* stably expressing YFP-CHC. Arrowheads indicate CCSs in blinking mode followed from their appearance at the PM until disappearance. Time is indicated in seconds at the left top corners, with 0.0 s indicating appearance of the pointed CCS. Scale bar, 1 um.

(F) CCS blinking time (time between appearance and disappearance of a CCS); n of blinking events = 20 for each genotype.

(G) VAEM/TIRF microscopy of hypocotyl epidermal cells in WT and *vap27-1/-3* stably expressing YFP-CHC. Arrowheads indicate the CCSs moving laterally before blinking. Each CCS is indicated by the same colored arrowhead overtime. Scale bar, 1 um.

(H) CCS velocity (lateral movement) (n CCSs analyzed = 716 for each genotype).

(I) Confocal images of leaf epidermal cells in WT and vap27-1/-3 stably expressing YFP-CHC. Arrowheads indicate TGN/EEs; arrows point to CCSs. Scale bar, 5 μ m.

(J) Number of CCSs/area (n areas = 50 for WT and 56 for vap27-1/-3).

(K) Proposed role in CME for VAP27-1 and VAP27-3 proteins at the EPCSs and TGN/EEs.

number of cytosolic CCSs is reduced in *vap27-1/-3*. Coupled with the reduction in the blinking and lateral movement of peripheral CCSs at the PM, these results

support an altered homeostasis of the endocytic membranes in conditions of a reduced cellular availability of VAP27-proteins, and are consistent the verified requirement of these ER proteins for the integrity of endocytic traffic (Figure 3).

DISCUSSION

Despite the reported close association of the ER with PM and endosomal organelles (Stefano et al., 2015; Wang et al., 2014), the identity of the factors bridging the ER with endocytic membranes are unknown in plant cells. Here, we established that the highly conserved VAP proteins, VAP27-1 and VAP27-3, which are localized to the bulk ER membrane and accumulate at the EPCSs (Wang et al., 2016), associate with clathrin and lipids enriched in endocytic membranes. We also demonstrated that the loss of the two VAP27-proteins partially compromises



endocytosis homeostasis, the dynamics of endocytic structures at the PM and plant growth. These findings support the model that the VAP27-proteins provide a molecular bridge between the ER and endocytic membranes (Figure 4K) and that such a role is necessary to maintain endocytic traffic. While a membrane-bridging function is consistent with the role of non-plant VAPs to bridge the ER and other organelles, including endosomes, mitochondria, and Golgi (Prinz, 2014), the interaction of VAPs with clathrin may underline a functional diversification of plant VAP27-proteins or differences in the plant CME compared to non-plant cells. Although the verified clathrin-VAP protein interaction may be indirect, we have shown a direct interaction of VAPs with PIPs, lipids abundant in endocytic membranes. The results of an interaction of VAPs with PIPs are in agreement with the recent findings that synaptotagmin SYT1, which partially co-localizes with VAP27-3 at the EPCSs (Pérez-Sancho et al., 2015; Siao et al., 2016), binds negatively charged PM phospholipids (Pérez-Sancho et al., 2015). Nonetheless, our results and earlier findings (Stefano et al., 2015) support also a temporary interaction of the ER with other endocytic membranes, such as the TGN/EEs (Figures 2E and S3D; Videos S1 and S2), besides the PM. In non-plant organisms, several PIPs, like the one found in our VAP27 interaction assay, are enriched at the endosomes, PM, and modulate late-stages of clathrin-coated pit formation (Simon et al., 2014). The evidence that some PIPs, such as PI4P, are enriched at the TGN/EEs (Simon et al., 2014) and interact with VAP27-proteins (Figure 1D) supports the possibility that a VAP-PI4P interaction may facilitate the association of the ER and TGN/EEs. Therefore, we propose that VAP27-proteins function as anchors between the ER and specific membrane sites where clathrin is recruited, through a direct interaction with PIPs. VAP27-proteins may interact also with other organelles, as supported by the evidence that these proteins interact with PI(3)P (Figure 1D), which can be found on LEs (Simon et al., 2014), and EPCSs and the bulk ER can be found in proximity of these organelles (Figure S2A) (Stefano et al., 2015).

A connection of VAP27-proteins with endocytic machinery (Figure 2) and endocytosis traffic (Figure 3) points to two models. First, the CME process is rate-limited by the assembly of the clathrin coat around the invagination or "pit" at the PM, which occurs over ~1-2 min (Loerke et al., 2009). Subsequently, departure of the clathrin-coated vesicle occurs on the timescale of \sim 10 s (Loerke et al., 2009). Clathrin is unable to bind the PM directly (Maldonado-Báez and Wendland, 2006). The verified interaction of clathrin with VAP27-proteins may be necessary for clathrin recruitment to the PM. Therefore, a loss of VAP27-proteins would slow down the maturation of the clathrin-coated vesicles and. consequently, their detachment. This is consistent with the observed reduced blinking of CCSs in the vap27 mutant compared to WT (Figure 4E). As a result, the endocytic traffic from the PM and the number of CCSs in the cytosol may be also reduced (Figures 4I and 4J). The latter part of this model postulates that the association of clathrin on newly formed CCSs released into the cytoplasm is long lived. Alternatively, or concomitantly with this model, the VAP27-proteins may be needed for the movement of CCSs and consequently for their trafficking function. Utilizing VAEM/TIRF microscopy, a linear lateral motion of cell-surface-associated CCSs parallel to the

PM has been visualized in multiple cell types, including plant cells (Rappoport and Simon, 2003; Wan et al., 2011). We found that the loss of VAP27-proteins did not affect the number of CCSs at the PM; however, their lateral movement was significantly reduced in the mutant compared to WT. In light of the verified influence of the ER streaming and ER membrane fluidity on the movement of endosomal organelles (Stefano et al., 2015), the loss of a membrane-anchored ER bridge with clathrin-associated endosomes could reduce the movement of CCSs in the cytosol and negatively their function as endocytic cargo carriers. As a result, not only endocytosis would be compromised, the number of endocytic structures in the cell would also be reduced due to inefficient recycling of endocytic effectors such as SNAREs and lipids. In mammalian cells, the movement the CCSs was found to be coincident with microtubules, and depolymerization of microtubules led to a reduction of the motility of these punctae (Rappoport et al., 2003). VAP27-proteins directly interact with microtubules (Wang et al., 2014). It has also been demonstrated that the movement of the plant ER depends at least partially on microtubules (Hamada et al., 2014). Based on these premises, the reduced movement of the CCSs verified in our work may be correlated to an interaction of VAP27-proteins with clathrin and microtubules. Therefore, in the absence of the VAP27-proteins, endocytic traffic may be slowed down due to the lack of efficient movement of the CCSs over microtubules and the ER network, which would be normally facilitated by VAP27-proteins serving as a bridge between the CCSs, ER membranes, and microtubules.

The TGN/EE is at the crossroad of both the biosynthetic and endocytic pathways, and clathrin is distributed to specific subdomains of the TGN/EE membranes (Ito et al., 2012; Konopka et al., 2008). Ultrastructural analyses revealed defects in the TGN/EE morphology (Figure S4G), indicating that the loss of VAP27-proteins compromises not only endocytic traffic at the PM but also the integrity of the TGN/EEs. The verified TGN/EE defects may be a consequence of disrupted endocytosis at the PM through an impairment of the anterograde traffic caused by the lack of recycling of trafficking machinery at the TGN/EEs. However, given the demonstrated association of the plant ER with endosomal membranes, including the TGN/EEs (Stefano et al., 2015), we propose that VAP27-proteins may also affect TGN/EE integrity directly. The loss of a clathrin-binding bridge between the ER and the TGN/EE membranes mediated by the VAPs may compromise the trafficking ability of the TGN/EEs, and as a consequence, lead to a morphological disruption of this organelle. A simple model in this respect could be that the interaction of the ER membrane with the TGN/EEs through VAPs may facilitate clathrin-coated vesicle formation through a VAP-mediated clathrin recruitment; alternatively, the ER/TGN interaction may facilitate clathrin vesicle maturation and budding from the TGN/EEs through "pulling" forces exerted by the ER through clathrin-interacting VAPs.

The two VAP27-proteins analyzed in our work belong to a family of four VAPs. Interrogating a mutant lacking all four VAP27-proteins will be necessary to test whether the two yet-untested VAP27-proteins are also involved in endocytosis. The viability of the *vap27-1/-3* mutant and the sequence similarity among the four VAP27-proteins suggest that they may share overlapping functions. Although the interactome of plant VAP-proteins is being

discovered (this work; see also Saravanan et al., 2009; Wang et al., 2014), the role of these proteins at organismal level had not been unraveled before this study. In this work, we have demonstrated that both proteins are involved in plant growth. Although we do not exclude that these VAPs may have additional roles in the cells, the growth phenotypes verified for vap27-1/-3 may be linked to a defective endocytosis, as demonstrated for other CME mutants (Collings et al., 2008; Stefano et al., 2015). VAP27-1 and VAP27-3 are known to heteromerize (Wang et al., 2014). Our results showing that the weight of the shoot and root of vap27-1/-3 is similar to either vap27-1 or vap27-3 are in line with VAP27-heteromerization in a functional complex. However, the evidence that, unlike vap27-3, deletion of VAP27-1 affects root elongation, and a deletion of VAP27-3, but not VAP27-1, affects root diameter, indicates that the two proteins have non-completely overlapping functions or interacting partners in root growth. These results support some degree of tissue specificity for the VAP27-proteins and suggest the possibility that VAP27-1 and VAP27-3 may form functional complexes with other VAP27-protein in roots.

A functional heterogeneity across plant EPCSs has been proposed based on the findings that the EPCSs labeled by synaptotagmin A (SYTA), another constituent of plant EPCSs, only partially overlap with VAP27-EPCSs (McFarlane et al., 2017; Siao et al., 2016). In our study, we have uncovered that the EPCSs marked by VAP27-proteins transiently associate with CCSs, and the association of CCSs with EPCSs does not occur simultaneously across all the EPCSs. These data indicate that the EPCSs interacting with clathrin represent a subpopulation of the cell's EPCSs. Therefore, our findings are in agreement with the evidence that the composition of plant EPCSs is heterogeneous (McFarlane et al., 2017; Siao et al., 2016) and support a diversification of the EPCSs, which likely underlies a functional specialization of these ER subdomains.

EXPERIMENTAL PROCEDURES

Cloning, Plant Material, and Growth Conditions

VAP27 and *CHC2* cDNAs were cloned into either pVKH18En6 or pEarlyGateway104 as CFP or vYFP fusions. For Y2H assays, VAP27-cytosolic domains were cloned into pBD42-AD or pGilda (Withers et al., 2012). For recombinant protein production, VAP27-cytosolic domains were cloned into pET28b or pGEX5x-1. Four-week-old *Nicotiana tabacum* (cv Petit Havana) plants grown at 25°C were used for transient expression (Batoko et al., 2000), with a bacterial OD₆₀₀ of 0.05. T-DNA lines were obtained from ABRC. Homozygous transgenic *A. thaliana* lines (Col-0 ecotype) expressing CHC2 were generated by floral dipping (Clough and Bent, 1998). *Arabidopsis* plants were germinated and grown at 21°C under 16 hr light/8 hr dark conditions. The list of primer sequences is provided in Table S1.

RNA Extraction, PCR, and Protein Blot Analyses

RNA extraction and qRT-PCR were performed as described previously (Stefano et al., 2012). One-week-old seedlings were harvested, homogenated, separated by SDS-PAGE, and blotted on nitrocellulose membrane (Renna et al., 2013). The blotted membrane was incubated with a GFP antibody (Abcam).

coIP and Proteomics Analyses

CoIP experiments were performed using the Dynabeads Protein A Immunoprecipitation kit (Thermo Fisher Scientific). Two-week-old *Arabidopsis* seedlings WT (CoI-0) or stably expressing VAP27-1-YFP, VAP27-3-YFP were homogenized in lysis buffer, and binding was performed as specified by the manufacturer's protocol. The eluate was collected and submitted for LC/MS/MS analysis.

Expression and Purification of Recombinant VAP27-Proteins

Recombinant VAP27-1 Δ TM and VAP27-3 Δ TM carrying a 6His-tag or GST-tag at the N terminus were expressed and purified as previously described (Stefano et al., 2006). Purified proteins were concentrated using Amicon ultra centrifugal filters and were stored at -80° C prior to use.

Yeast Two-Hybrid Assays

Yeast two-hybrid (Y2H) assays were performed as previously described (Withers et al., 2012) using GAL4 system (Clontech, Mountainview, CA). The assay was repeated at least three times with consistent results.

Protein Lipid Overlay Assay

Lipid binding assays were performed according to the manufacturers' instructions (Echelon Biosciences, Salt Lake City). VAP27-1 Δ TM-6HIS and GST-VAP27-3 Δ TM were detected using anti-HIS serum (Santa Cruz Biotechnology) and anti-GST serum (Thermo Fisher Scientific), respectively.

Confocal Laser Scanning Microscopy and VAEM-TIRF

Confocal laser scanning microscopy (CLSM) was performed using an inverted Nikon A1Rsi microscope equipped with a 60 × objective (Apo Oil λS DIC N2). CFP and YFP were excited using 443 and 514 nm laser lines, respectively; signals were collected using 485/35, and 580/40 filter cubes. For FRET experiments, the donor molecule was excited at 443 nm and fluorescence was collected at 468–503 nm; the acceptor was excited at 514 nm and the fluorescent signal was collected between 570 and 620 nm. VAEM/TIRF analyses were performed on a Nikon A1Rsi system equipped with a CFI Apo TIRF 100 × NA1.49 oil immersion objective and a Andor iXon camera (Du 897 Ultra). Etiolated hypocotyls of 6-day-old seedlings were used for the analyses.

Drug and Dye Treatments

Arabidopsis seedlings were incubated with 2 μ M FM4-64 and observed after 5 min, 15 min, or 1 hr. For BFA treatment, the seedlings were first incubated with 2 μ M FM4-64 then treated in 50 μ M BFA.

Transmission Electron Microscopy

Leaves from 2-week-old *Arabidopsis* plants embedded and ultrathin sections (70-nm thick) were cut on an RMC ultramicrotome (RMC, Tucson, AZ), and then mounted on grids. TEM images analysis were taken with a JEOL100 CXII instrument (Japan Electron Optics Laboratories).

Statistical Analyses

Statistical analysis one-way ANOVA with Tukey's post-tests was performed for root length and for weight measurements, while Student's t test was performed for all other analyses. Error bars in Figures 3B, 3D, 4A, 4J, S4C–S4F, S4H, and S4I indicate SEM. Boxplot whiskers in Figures 4D, 4F, 4H, and S4J indicate min and max. ***p < 0.001; **0.01 > p < 0.01; *0.01 > p < 0.05; n.s., not significant. Additional experimental details can be found in the Supplemental Information.

SUPPLEMENTAL INFORMATION

Supplemental Information includes Supplemental Experimental Procedures, four figures, one table, and two videos and can be found with this article online at https://doi.org/10.1016/j.celrep.2018.04.091.

ACKNOWLEDGMENTS

We acknowledge support by the Chemical Sciences, Geosciences and Biosciences Division, Office of Basic Energy Sciences, Office of Science, U.S. Department of Energy (DE-FG02-91ER20021) and the National Science Foundation (MCB1714561) and AgBioResearch to FB.



AUTHOR CONTRIBUTIONS

G.S., L.R., and F.B. designed the research and wrote the manuscript. G.S., L.R., C.W., J.G., and K.Z. performed the experiments.

DECLARATION OF INTERESTS

The authors declare no competing interests.

Received: July 24, 2017 Revised: March 26, 2018 Accepted: April 20, 2018 Published: May 22, 2018

REFERENCES

Alpy, F., Rousseau, A., Schwab, Y., Legueux, F., Stoll, I., Wendling, C., Spiegelhalter, C., Kessler, P., Mathelin, C., Rio, M.C., et al. (2013). STARD3 or STARD3NL and VAP form a novel molecular tether between late endosomes and the ER. J. Cell Sci. 126, 5500-5512.

Batoko, H., Zheng, H.Q., Hawes, C., and Moore, I. (2000). A rab1 GTPase is required for transport between the endoplasmic reticulum and golgi apparatus and for normal golgi movement in plants. Plant Cell 12, 2201-2218.

Clough, S.J., and Bent, A.F. (1998). Floral dip: a simplified method for Agrobacterium-mediated transformation of Arabidopsis thaliana. Plant J. 16,

Collings, D.A., Gebbie, L.K., Howles, P.A., Hurley, U.A., Birch, R.J., Cork, A.H., Hocart, C.H., Arioli, T., and Williamson, R.E. (2008). Arabidopsis dynamin-like protein DRP1A: a null mutant with widespread defects in endocytosis, cellulose synthesis, cytokinesis, and cell expansion. J. Exp. Bot. 59, 361-376.

Doyle, S.M., Haeger, A., Vain, T., Rigal, A., Viotti, C., Langowska, M., Ma, Q., Friml, J., Raikhel, N.V., Hicks, G.R., et al. (2015). An early secretory pathway mediated by GNOM-LIKE 1 and GNOM is essential for basal polarity establishment in Arabidopsis thaliana. PNAS 112, E806-815.

Fan, L., Hao, H., Xue, Y., Zhang, L., Song, K., Ding, Z., Botella, M.A., Wang, H., and Lin, J. (2013). Dynamic analysis of Arabidopsis AP2 σ subunit reveals a key role in clathrin-mediated endocytosis and plant development. Development 140, 3826-3837.

Fan, L., Li, R., Pan, J., Ding, Z., and Lin, J. (2015). Endocytosis and its regulation in plants. Trends Plant Sci. 20, 388-397.

Gadeyne, A., Sánchez-Rodríguez, C., Vanneste, S., Di Rubbo, S., Zauber, H., Vanneste, K., Van Leene, J., De Winne, N., Eeckhout, D., Persiau, G., et al. (2014). The TPLATE adaptor complex drives clathrin-mediated endocytosis in plants. Cell 156, 691-704.

Hamada, T., Ueda, H., Kawase, T., and Hara-Nishimura, I. (2014). Microtubules contribute to tubule elongation and anchoring of endoplasmic reticulum, resulting in high network complexity in Arabidopsis. Plant Physiol. 166, 1869-1876.

Ito, E., Fujimoto, M., Ebine, K., Uemura, T., Ueda, T., and Nakano, A. (2012). Dynamic behavior of clathrin in Arabidopsis thaliana unveiled by live imaging. Plant J. 69. 204-216.

Konopka, C.A., Backues, S.K., and Bednarek, S.Y. (2008). Dynamics of Arabidopsis dynamin-related protein 1C and a clathrin light chain at the plasma membrane. Plant Cell 20, 1363-1380.

Lam, S.K., Cai, Y., Tse, Y.C., Wang, J., Law, A.H., Pimpl, P., Chan, H.Y., Xia, J., and Jiang, L. (2009). BFA-induced compartments from the Golgi apparatus and trans-Golgi network/early endosome are distinct in plant cells. Plant J. 60.865-881.

Lev, S., Ben Halevy, D., Peretti, D., and Dahan, N. (2008). The VAP protein familv: from cellular functions to motor neuron disease. Trends Cell Biol. 18.

Loerke, D., Mettlen, M., Yarar, D., Jaqaman, K., Jaqaman, H., Danuser, G., and Schmid, S.L. (2009). Cargo and dynamin regulate clathrin-coated pit maturation. PLoS Biol. 7, e57.

Maldonado-Báez, L., and Wendland, B. (2006). Endocytic adaptors: recruiters, coordinators and regulators. Trends Cell Biol. 16, 505-513.

McFarlane, H.E., Lee, E.K., van Bezouwen, L.S., Ross, B., Rosado, A., and Samuels, A.L. (2017). Multiscale structural analysis of plant ER-PM contact sites. Plant Cell Physiol. 58, 478-484.

McMahon, H.T., and Boucrot, E. (2011). Molecular mechanism and physiological functions of clathrin-mediated endocytosis. Nat. Rev. Mol. Cell Biol. 12, 517-533.

Ortiz-Morea, F.A., Savatin, D.V., Dejonghe, W., Kumar, R., Luo, Y., Adamowski, M., Van den Begin, J., Dressano, K., Pereira de Oliveira, G., Zhao, X., et al. (2016). Danger-associated peptide signaling in Arabidopsis requires clathrin. Proc. Natl. Acad. Sci. USA 113, 11028-11033.

Paciorek, T., Zazímalová, E., Ruthardt, N., Petrásek, J., Stierhof, Y.D., Kleine-Vehn, J., Morris, D.A., Emans, N., Jürgens, G., Geldner, N., and Friml, J. (2005). Auxin inhibits endocytosis and promotes its own efflux from cells. Nature 435, 1251-1256

Pérez-Sancho, J., Vanneste, S., Lee, E., McFarlane, H.E., Esteban Del Valle, A., Valpuesta, V., Friml, J., Botella, M.A., and Rosado, A. (2015). The Arabidopsis synaptotagmin1 is enriched in endoplasmic reticulum-plasma membrane contact sites and confers cellular resistance to mechanical stresses. Plant Physiol. 168, 132-143.

Prinz, W.A. (2014). Bridging the gap: membrane contact sites in signaling, metabolism, and organelle dynamics. J. Cell Biol. 205, 759-769.

Puertollano, R., Randazzo, P.A., Presley, J.F., Hartnell, L.M., and Bonifacino, J.S. (2001). The GGAs promote ARF-dependent recruitment of clathrin to the TGN. Cell 105, 93-102.

Rappoport, J.Z., and Simon, S.M. (2003). Real-time analysis of clathrin-mediated endocytosis during cell migration. J. Cell Sci. 116, 847-855.

Rappoport, J.Z., Taha, B.W., and Simon, S.M. (2003). Movement of plasmamembrane-associated clathrin spots along the microtubule cytoskeleton. Traffic 4, 460-467.

Renna, L., Stefano, G., Majeran, W., Micalella, C., Meinnel, T., Giglione, C., and Brandizzi, F. (2013). Golgi traffic and integrity depend on N-myristoyl transferase-1 in Arabidopsis. Plant Cell 25, 1756-1773.

Robinson, M.S. (2015). Forty years of clathrin-coated vesicles. Traffic 16, 1210-1238.

Saravanan, R.S., Slabaugh, E., Singh, V.R., Lapidus, L.J., Haas, T., and Brandizzi, F. (2009). The targeting of the oxysterol-binding protein ORP3a to the endoplasmic reticulum relies on the plant VAP33 homolog PVA12. Plant J. 58, 817-830.

Siao, W., Wang, P., Voigt, B., Hussey, P.J., and Baluska, F. (2016). Arabidopsis SYT1 maintains stability of cortical endoplasmic reticulum networks and VAP27-1-enriched endoplasmic reticulum-plasma membrane contact sites. J. Exp. Bot. 67, 6161-6171.

Simon, M.L., Platre, M.P., Assil, S., van Wijk, R., Chen, W.Y., Chory, J., Dreux, M., Munnik, T., and Jaillais, Y. (2014). A multi-colour/multi-affinity marker set to visualize phosphoinositide dynamics in Arabidopsis. Plant J. 77, 322-337.

Stefan, C.J., Manford, A.G., Baird, D., Yamada-Hanff, J., Mao, Y., and Emr, S.D. (2011). Osh proteins regulate phosphoinositide metabolism at ER-plasma membrane contact sites. Cell 144, 389-401.

Stefan, C.J., Manford, A.G., and Emr, S.D. (2013). ER-PM connections: sites of information transfer and inter-organelle communication. Curr. Opin. Cell Biol. 25, 434-442,

Stefano, G., Renna, L., Hanton, S.L., Chatre, L., Haas, T.A., and Brandizzi, F. (2006). ARL1 plays a role in the binding of the GRIP domain of a peripheral matrix protein to the Golgi apparatus in plant cells. Plant Mol. Biol. 61, 431-449. Stefano, G., Renna, L., Moss, T., McNew, J.A., and Brandizzi, F. (2012). In Arabidopsis, the spatial and dynamic organization of the endoplasmic reticulum and Golgi apparatus is influenced by the integrity of the C-terminal domain of RHD3, a non-essential GTPase. Plant J. 69, 957-966.

Stefano, G., Renna, L., Lai, Y., Slabaugh, E., Mannino, N., Buono, R.A., Otegui, M.S., and Brandizzi, F. (2015). ER network homeostasis is critical for plant endosome streaming and endocytosis. Cell Discov. 1, 15033.



Ueda, T., Uemura, T., Sato, M.H., and Nakano, A. (2004). Functional differentiation of endosomes in Arabidopsis cells. Plant J. 40, 783–789.

Viotti, C., Bubeck, J., Stierhof, Y.D., Krebs, M., Langhans, M., van den Berg, W., van Dongen, W., Richter, S., Geldner, N., Takano, J., et al. (2010). Endocytic and secretory traffic in Arabidopsis merge in the trans-Golgi network/early endosome, an independent and highly dynamic organelle. Plant Cell 22, 1344–1357.

Voigt, B., Timmers, A.C., Samaj, J., Hlavacka, A., Ueda, T., Preuss, M., Nielsen, E., Mathur, J., Emans, N., Stenmark, H., et al. (2005). Actin-based motility of endosomes is linked to the polar tip growth of root hairs. Eur. J. Cell Biol. 84, 609–621.

Wan, Y., Ash, W.M., 3rd, Fan, L., Hao, H., Kim, M.K., and Lin, J. (2011). Variable-angle total internal reflection fluorescence microscopy of intact cells of Arabidopsis thaliana. Plant Methods 7, 27.

Wang, C., Yan, X., Chen, Q., Jiang, N., Fu, W., Ma, B., Liu, J., Li, C., Bednarek, S.Y., and Pan, J. (2013). Clathrin light chains regulate clathrin-mediated trafficking, auxin signaling, and development in Arabidopsis. Plant Cell *25*, 499–516.

Wang, P., Hawkins, T.J., Richardson, C., Cummins, I., Deeks, M.J., Sparkes, I., Hawes, C., and Hussey, P.J. (2014). The plant cytoskeleton, NET3C, and VAP27 mediate the link between the plasma membrane and endoplasmic reticulum. Curr. Biol. 24, 1397–1405.

Wang, C., Zhu, M., Duan, L., Yu, H., Chang, X., Li, L., Kang, H., Feng, Y., Zhu, H., Hong, Z., and Zhang, Z. (2015). Lotus japonicus clathrin heavy Chain1 is associated with Rho-Like GTPase ROP6 and involved in nodule formation. Plant Physiol. *167*, 1497–1510.

Wang, P., Richardson, C., Hawkins, T.J., Sparkes, I., Hawes, C., and Hussey, P.J. (2016). Plant VAP27 proteins: domain characterization, intracellular localization and role in plant development. New Phytol. *210*, 1311–1326.

Wang, P., Hawes, C., and Hussey, P.J. (2017). Plant endoplasmic reticulumplasma membrane contact sites. Trends Plant Sci. 22, 289–297.

Withers, J., Yao, J., Mecey, C., Howe, G.A., Melotto, M., and He, S.Y. (2012). Transcription factor-dependent nuclear localization of a transcriptional repressor in jasmonate hormone signaling. Proc. Natl. Acad. Sci. USA *109*, 20148–20153.